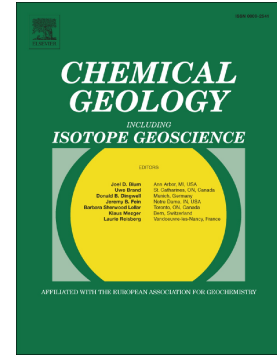


Journal Pre-proof

U-series histories of magmatic volatile phase and enclave development at Soufrière Hills Volcano, Montserrat

Lucy McGee, Mark Reagan, Simon Turner, Steve Sparks, Heather Handley, Rosa Didonna, Kim Berlo, Sarah Hansen, Jenni Barclay



PII: S0009-2541(20)30496-4

DOI: <https://doi.org/10.1016/j.chemgeo.2020.119957>

Reference: CHEMGE 119957

To appear in: *Chemical Geology*

Received date: 24 March 2020

Revised date: 21 October 2020

Accepted date: 22 October 2020

Please cite this article as: L. McGee, M. Reagan, S. Turner, et al., U-series histories of magmatic volatile phase and enclave development at Soufrière Hills Volcano, Montserrat, *Chemical Geology* (2020), <https://doi.org/10.1016/j.chemgeo.2020.119957>

This is a PDF file of an article that has undergone enhancements after acceptance, such as the addition of a cover page and metadata, and formatting for readability, but it is not yet the definitive version of record. This version will undergo additional copyediting, typesetting and review before it is published in its final form, but we are providing this version to give early visibility of the article. Please note that, during the production process, errors may be discovered which could affect the content, and all legal disclaimers that apply to the journal pertain.

© 2020 Published by Elsevier.

U-series histories of magmatic volatile phase and enclave development at Soufrière Hills Volcano, Montserrat

Lucy McGee^{1,2}, Mark Reagan³, Simon Turner¹, Steve Sparks⁴, Heather Handley¹, Rosa Didonna¹, Kim Berlo⁵, Sarah Hansen³ and Jenni Barclay⁶

¹ Department of Earth and Environmental Sciences, Macquarie University, Sydney, Australia

² Department of Earth Sciences, University of Adelaide, Adelaide, Australia,

³ Department of Earth and Environmental Sciences, The University of Iowa, Iowa, USA,

⁴ School of Earth Sciences, University of Bristol, Bristol, UK

⁵ Department of Earth and Planetary Sciences, McGill University, Montreal, Canada

⁶ School of Environmental Science, University of East Anglia, Norwich, UK

*Corresponding author: lucy.mcgee@adelaide.edu.au

Abstract

Injection of volatile-rich mafic magma prior to an eruption may trigger episodes of volcanism and can act to transfer metals from depth. However, petrologic knowledge of the timescales from mafic injection to eruption have thus far been focussed on mineral-scale studies of chemical zoning patterns. The study of mafic enclaves dispersed within eruption products can provide insights into the interaction between deep and shallow reservoirs. We combine ²³⁸U-²³⁰Th-²²⁶Ra-²¹⁰Pb isotope data with trace element concentrations across the interface of two contrasting mafic enclaves in contact with their host andesite from the 2010 eruption at Soufrière Hills Volcano (SHV), Montserrat to investigate the history of mass exchange between the mafic enclave and the andesite host. The application of these time-sensitive isotopes highlights complexities in the transfer of volatiles and metal elements between magmas and the enclaves' potential as eruption triggers. The enclaves exhibit (²¹⁰Pb/²²⁶Ra)₀ ratios > 1 consistent with volatile input to the subsurface plumbing system a few decades prior to eruption. Samples of the andesitic host, however, which make up the bulk of the eruptive products, have (²¹⁰Pb/²²⁶Ra)₀ ≤ 1 suggesting no net volatile gain in the decades leading up to eruption, or that melt-volatile interaction is on a timescale unresolvable by ²¹⁰Pb-²²⁶Ra systematics (i.e. <2 years). Variations in trace elements such as Cu, Pb and Ba show loss of a magmatic volatile phase and transport of metals within the deeper part of the plumbing system during differentiation of magmas feeding SHV. Our results do not support that volatile transfer into the andesite via enclaves is a direct trigger of explosive eruptions although the enclaves are likely syn-eruptively formed. ²³⁸U-²³⁰Th-²²⁶Ra-²¹⁰Pb and trace element systematics at SHV support a role for fresh magma influx during periods of unrest, but long-term accumulation of the andesite.

Keywords

Soufrière Hills Volcano; ^{226}Ra - ^{210}Pb ; Enclaves; Eruption triggers; Magmatic Volatile Phase; Copper

1. Introduction

Models of subsurface magmatic plumbing systems are becoming increasingly complex with advances in geophysical and geochemical studies from the regional scale of the whole volcano down to the individual crystal scale (Sparks et al., 2019). Detailed geochemical studies of the individual components of a magmatic system (e.g. volatiles, crystals, melts) can provide information on their interactions with one another and over what timescales, revealing important detail of the volcanic process from mafic recharge at depth to explosive eruption and outgassing at the surface. Micro-scale observations such as crystal 'stratigraphy' (e.g. Santorini, Marin et al., 2008 and Quizapu, Ruprecht and Bachmann, 2010), and glass composition studies (e.g. Eyjafjallajökull 2010 (Sigmarsson et al., 2011) and Pinatubo 1991 (Pallister et al., 1992)) have provided insight into these processes. Although these approaches can constrain timing of mafic injection, they provide less constraint on the role of volatiles in driving recharge or explosive eruption. Understanding the whole magmatic and volcanic system from source to surface is of great importance at active volcanoes which are constantly monitored. Some silicic explosive eruptions may be triggered by injection of mafic magma causing magma mixing, re-heating, convection, the transfer of volatiles and then vesiculation. These magma chamber processes can subsequently lead to overpressure and induce an explosive eruption (e.g. Sparks et al., 1977). The injection of fresh, mafic magma at arc volcanoes also provides a source of sulphur and halogens which can complex with metal elements such as copper (e.g. Nadeau et al., 2016). Answering questions regarding the transport of metals and their eventual enrichment in the subsurface is becoming increasingly critical as green industry and stringent energy requirements become more important.

Uranium series radionuclide analyses can be applied to young volcanic products to investigate the histories of interactions between magmas and volatile phases (Bourdon et al., 2003). The ^{226}Ra - ^{210}Pb pair are particularly useful because an intermediary daughter, ^{222}Rn (half-life ($t_{1/2}$) = 3.8 days), will preferentially partition from magmas into an associated magmatic volatile phase (MVP). In addition, ^{210}Pb ($t_{1/2}$ = 22.6 years) may preferentially partition into the MVP along with common Pb if it is sufficiently saline (e.g. Rusk et al., 2004). Thus, a $(^{210}\text{Pb}/^{226}\text{Ra})_0$ activity ratio which differs from one in recently erupted volcanic rocks is a strong indicator of volatile loss or gain prior to eruption (Berlo and Turner, 2010; Gauthier and Condomines, 1999).

We present data on trace element and ^{238}U - ^{230}Th - ^{226}Ra - ^{210}Pb variations across mafic enclave-andesite host interfaces to investigate the role of mafic magma recharge and volatile transfer beneath an active arc volcano. The most recent eruption at Soufrière Hills Volcano, Montserrat (SHV) in January-February 2010 provides a unique opportunity for detailed investigation of volatile and metal transport via mafic enclaves, and the potential of this process as an eruption trigger.

2. The 1995-2010 AD eruption of Soufrière Hills volcano and the significance of enclave formation

From July 1995 to February 2010 SHV underwent five eruptive phases (Phases I-V) characterised by dome growth alternating with repose periods. All andesitic pyroclastic flow deposits formed by dome collapse contain mafic enclaves (1-7%) resulting from magmatic interactions and which are interpreted as ultimately due to recharge of the magmatic system (Barclay et al., 2010). Details of the eruptions, monitoring and petrology of the volcanic rocks are summarised in Wadge et al. (2014). A prominent feature of SHV is its large SO_2 plume and continued outgassing throughout the hiatuses and since February 2010. This is likely due to the presence of pathways through the crystal mush which allows for transport of volatiles provided by multiple cycles of underplating mafic magmas (Edmonds and Woods, 2018). A ^{210}Pb - ^{226}Ra study of bulk enclaves and andesites spanning the entire duration of the eruption inferred the cessation of mafic input and subsequent fresh volatile supply towards the end of Phase II (McGee et al., 2019), consistent with petrologic observations of the enclaves over time by Plail et al. (2018).

The formation of mafic enclaves within silicic host rocks is controlled by rheological and density contrasts developed between mixing magmas following heat exchange (Sparks and Marshall, 1986). Large viscosity contrasts favour enclave formation, although disaggregation of enclaves is also common (Coombs et al., 2003; Ubide et al., 2014) and is observed at SHV (Humphreys et al., 2009). Three main mechanisms of formation and incorporation of mafic enclaves have been suggested: (1) forced injection by dyking followed by convection (Bacon, 1986; Eichelberger and Izbekov, 2000); (2) the development of gravitational instabilities due to accumulation of volatiles within the mafic magma (Bacon, 1986; Coombs et al., 2003; Edmonds et al., 2015; Kayzar et al., 2009; Thomas and Tait, 1997), and (3) syn-eruptive formation of enclaves, where hybridised enclaves are rapidly incorporated into their host during ascent and eruption (Cioni et al., 1995; Plail et al., 2018; Suzuki et al., 2013). The addition of mafic material at depth is recognised as a means of growing and maintaining the eruptive mass of the magma reservoir (Cioni et al., 1995; Plail et al., 2018). Importantly, eruption triggers could also be external, although all three mechanisms described here provide a means of introducing heat, volatiles and volume into the overlying magma reservoir.

The interface between the mafic and silicic magmas is a critical zone for understanding enclave formation, their potential as an eruption trigger, and the transfer of volatiles and elements that may occur. Here we examine two texturally different volcanic rock samples that are equally abundant at SHV (Plail et al., 2014a) collected from the products emplaced during the final dome collapse of February 2010. Although enclaves occur in andesitic material throughout all five eruptive phases at SHV we focus on the last eruption of Phase V to investigate the most recent mass exchange to occur at the volcano. One sample is a non-vesicular enclave and was serially sectioned across the enclave-host andesite boundary (**Fig. 1A**). The other sample contains a highly vesicular enclave interior and was cut into representative sections (vesicular enclave, non-vesicular enclave, andesite host, **Fig. 1B**).

3. Methods

Samples of clast material from pyroclastic flow deposits emplaced in February 2010 (MT35 and MT75, **Fig. 1**) were cut with a precision diamond saw. Polished thin sections were made of small portions of the samples across the enclave-andesite interface, the remaining sample was cleaned in distilled water, dried, crushed and powdered in a agate mill. All data, blanks, duplicates, and standards are presented in the **online appendix**. The data presented in figures are shown in **Table 1**.

3.1. X-ray mapping

Micro XRF maps of major and trace element abundances were produced using a Bruker M4 Tornado on polished thin sections. The instrument is equipped with a Rh X-ray tube (excited at 50 keV and 200 mA) and two Bruker 30mm² X-flash SDD EDS detectors. The beam diameter was 20 mm, the pixel size was 35 mm per pixel with a dwell time of 10 ms and the instrument was scanning continuously at a rate of 100 mm/s. The M4 Tornado's software (HyperMap) elaborated the spectroscopic information obtained.

3.2. Whole rock trace element geochemistry

Approximately 100 mg of each sample was digested using a 1:1 mixture of HF (Merck, Suprapur grade) and Teflon distilled HNO₃ (Merck) at 120°C for 24 hours, then dried down and repeated. Samples were then digested in a mixture of 2 ml HF (Merck Suprapur) and 10 drops of HClO₄ (Merck Suprapur) overnight and dried down gradually to remove fluoride complexes. A further digest in 6N HCl and then 6N HNO₃ was performed before samples were dissolved in a 2% HNO₃ + 0.5% HF for analysis. Samples were spiked with 20 µL of a mixed solution containing ⁶Li, As, Rh, In and Bi in 2% HNO₃ to monitor instrument drift throughout the analytical session. Trace elements were analysed by Inductively Coupled Plasma Mass Spectrometry (ICP-MS) on an Agilent 7500cs at Macquarie

Geoanalytical (MQGA) at Macquarie University. USGS rock standard BCR-2 was used for calibration and BIR-1 and BHVO-2 were analysed at 1:1000, 1:2000, and 1:5000 dilutions as unknowns to assess data accuracy. All standard data and a method blank are reported in the **online appendix**. Most elements were measured to within 5% of GeoRem preferred values (2016), all other relevant elements were within 10% with the exceptions of Cu (8% in BIR-1, 11% in BHVO-2), Ta (12% in BIR-1 at 0.03 ppm, 3% in BHVO-2), Pb (57% in BIR-1, 2.6% in BHVO-2) and Th (11.6% in BIR-1 at 0.03 ppm, 1.3% in BHVO-2). Maximum error bars based on this accuracy are included in relevant figures. Internal precision based on repeat analyses of standards at the beginning and end of the analytical session is <4% for all elements and mostly better than 1.5%.

3.3. Whole rock U-Th-Ra-Pb isotopes

Approximately 300 mg of each sample was spiked with a mixed ^{235}U - ^{229}Th and ^{228}Ra spike and digested following conventional methods. U and Th were extracted from a single pass through AG1-X8 resin and analysed by multi collector (MC)-ICP-MS (Nu Instruments) at MQGA. Further separation through two AG50W-X8 columns, a Ln-spec column and a Sr-spec column purified the Ra fraction, which was analysed by Thermal Ionisation Mass Spectrometry (Thermo Finnigan Triton) also at MQGA. ^{210}Pb was analysed using ^{210}Po as a proxy. A 2 g aliquot of sample powder was digested and Po eluted from the sample matrix using warm 0.5N HNO_3 on a column of AG1-X8 cationic resin. Po was auto-plated onto silver discs using a magnetic hotplate and alpha radiation counted on an Ametek Alpha Counter for approximately 10 days. Post-analysis processing converted ^{210}Po to initial ^{210}Pb based on the age of the samples and the half-lives involved ($^{210}\text{Po} = 138$ days, $^{210}\text{Pb} = 22.6$ years, Bourdon et al., 2003). McGee et al. (2019) present full details of the analytical procedures employed. All U-Th-Ra and the ^{210}Pb for sample MT35 were analysed at MQGA. ^{210}Pb for sample MT75 was analysed at the University of Iowa. Two samples were duplicated for ^{226}Ra concentrations using a newly processed and calibrated ^{228}Ra spike at MQGA and these reproduced to better than 1% from the original value. One sample was duplicated for ^{210}Po concentration at MQGA and reproduced to within 7% of the original value. The standard TML (Table Mountain Latite) and USGS rock standard BCR-2 were run for U-Th-Ra isotopes and the data are compared to the compilation of Scott et al. (2019). The USGS rock standards BCR-2 and RGM-2 were run for ^{210}Po analyses and compared to the analyses reported in Reagan et al. (2017). U-Th isotopes and concentrations for standards reproduce better than 3%, ^{226}Ra concentration and ($^{226}\text{Ra}/^{230}\text{Th}$) ratios reproduce better than 5% and ^{210}Po concentrations reproduce better than 1.5% relative to the preferred values. Throughout the paper parentheses denote activity ratios.

3.4. Whole rock volatile data

Whole rock contents of carbon, sulphur and nitrogen were analysed on rock powder aliquots on an Elementar VARIO EL Cube at MQGA. USGS rock standards BCR-2 and AGV-2 were run throughout each analytical session and are compared to both literature values (where available) and long-term reproducibility within MQGA. In the following plots the range of values obtained for multiple aliquots of each sample are plotted, as this is greater than the offset from the standards. All standards are shown in the **online appendix**.

4. Results

4.1. Petrography

Samples MT35 and MT75 contain similar mineral assemblages for both host andesite and basaltic andesite enclave portions: the main minerals are plagioclase + orthopyroxene + amphibole and Fe-Ti oxides in decreasing order of abundance. Cross polarised light views of the samples are shown in **Figure 2**, and detailed X-ray maps of a section from both MT35 and MT75 are shown in **Figure 3** showing Al (red), Ca (green) and Fe (blue) abundances. Ranges of values for anorthite [$An = 100 \times \text{molar Ca}/(\text{Na}+\text{Ca}+\text{K})$] and MgO are based on unpublished on-going work on plagioclase by the authors.

Sample MT35 (**Fig. 1A**) is a porphyritic andesite and part of a basaltic andesitic enclave (defined as “Type A” by Plail et al. 2014a). In the andesitic host, plagioclase is the most abundant phase and has a range of textures (patchy, oscillatory zoning and sieve-textured). Plagioclase core compositions are An_{45-75} , with MgO contents from about 0.01 to 0.04 wt%, while rims are $>An_{70}$ and tend to have higher MgO than the cores. Orthopyroxene phenocrysts are unzoned or have a thin rim ($<10 \mu\text{m}$) of clinopyroxene. Amphibole is unreacted or sometimes contains inclusions of plagioclase and oxides. Quartz is present and has reaction rims of clinopyroxene and magnetite. Apatite and rare zircon are also present. The groundmass of the host andesite is dominated by plagioclase with microlites of orthopyroxene, clinopyroxene, Fe-Ti oxides, glass and rare vesicles also present. In the enclave, orthopyroxene occurs as single isolated crystals or as glomerocrysts (up to 8 mm), some with reaction rims of clinopyroxene. Reacted large amphibole, quartz with or without reaction rims of clinopyroxene (up to 2 mm in size) and Fe-Ti oxides are in lower abundance than in the andesite portion. Accessory minerals are apatite and rare zircon. The groundmass of the enclave is diktytaxitic with euhedral laths of plagioclase, amphibole and pyroxene, and bounding crystal margins.

Sample MT75 (**Fig. 1B**) is an andesite containing a part of an enclave defined as composite (“Type C”, Plail et al., 2014a). Plagioclase is the dominant phase with textures and compositions similar to MT35: phenocrysts (up to ~ 3 mm in size), with core compositions of An_{50-55} and MgO 0.01-0.02 wt%

and with rims of An₇₀₋₈₅ and MgO up to 0.1 wt%. Orthopyroxene crystals are unzoned. Amphibole is unreacted and magnetite is also present. Quartz is not present in the host andesite. The andesite groundmass is dominated by microlites of plagioclase, orthopyroxene, clinopyroxene, Fe-Ti oxides and glass. The enclave portion shows two different textural zones. The zone in contact with the andesite ('non-vesicular enclave' in **Figure 1B**) has a higher abundance of plagioclase, orthopyroxene and amphibole phenocrysts presumably inherited from the host andesite that show disequilibrium textures (Plail et al. 2014; sieve-textured plagioclase, amphiboles with broken down rims, 'older' crystals in **Figure 2**) and low vesicularity. The diktytaxitic groundmass is composed of plagioclase, orthopyroxene, clinopyroxene, amphibole and glass, similar in texture to the basaltic andesitic enclave in MT35 (**Figs. 2-3**). The other, interior, zone ('vesicular enclave' on **Figure 1B**) is characterised by rare inherited phenocrysts of plagioclase, orthopyroxene and amphibole in a seriate-textured groundmass of euhedral plagioclase, clinopyroxene and amphibole. The higher vesicularity of the interior part of MT75 can be seen on the X-ray map in **Figure 3**.

4.2. Trace element and volatile data

All samples have incompatible trace element patterns that display a typical volcanic arc trend of relative enrichment in fluid mobile elements such as U, Pb and Sr and depletions in immobile elements such as Nb, Ta and Ti relative to the rare earth elements (REE). The mafic enclaves are similar to basalt samples from the South MHV eruption (Zellmer et al. 2003a), although the andesites are more enriched in the most incompatible elements (**Fig. 4**). All andesite samples have approximately double the concentration of highly incompatible trace elements (Rb, Ba, Th, U and the light REE) compared to the enclaves (**Figs. 4-5**), reflecting the more evolved nature of the andesite. Concentrations of several metals (Pb and Zn) and Sr, however, have similar abundances in both enclave portion and andesitic host of each sample (**Figs. 4-5, Table 1**). Cu is depleted in the andesite compared with the enclaves. Heavy REE concentrations are similar in all samples, with the exception of one more enriched MT35 enclave sample.

Whole rock S concentrations range from 24 to 62 ppm in MT35 and 32 to 72 ppm in MT75 (**Fig. 5**). The highest values are in MT35-B (enclave) and MT75-B (vesicular enclave) (see full dataset in the **online appendix**). C and N data show little variation except for anomalously high carbon values in sample MT75-C (**Fig. 5**).

4.3. U-series data

The U-series data largely lie within the range of previous bulk andesite and enclave data from the 1995-2010 eruption (McGee et al. 2019, **Fig. 6**). All samples have ($^{234}\text{U}/^{238}\text{U}$) ratios within error of or very close to equilibrium (**Table 1**). Andesite samples analysed here have slight U-excesses (lie to the right of the equiline in **Fig. 6A**; ($^{230}\text{Th}/^{238}\text{U}$) = 0.98-0.99) and equilibrium ($^{226}\text{Ra}/^{230}\text{Th}$) ratios (**Figs. 6A-B**). These andesites also have ^{210}Pb - ^{226}Ra equilibrium or small ^{210}Pb -deficits ($(^{210}\text{Pb}/^{226}\text{Ra})_0 < 1$). The serial enclave samples have more significant U-excesses ($(^{230}\text{Th}/^{238}\text{U}) = 0.91-0.97$) and moderate ^{226}Ra -excesses ($(^{226}\text{Ra}/^{230}\text{Th}) = 1.07-1.81$). A majority of these samples have ^{210}Pb -excesses ($(^{210}\text{Pb}/^{226}\text{Ra})_0$ up to 1.4) or have ($^{210}\text{Pb}/^{226}\text{Ra})_0$ values within error of equilibrium (**Fig. 6C**).

In detail, all enclave slices from MT35 have ^{210}Pb -excesses ($(^{210}\text{Pb}/^{226}\text{Ra})_0 = 1.3$ to 1.4), ($^{226}\text{Ra}/^{230}\text{Th}$) = ~ 1.2 , and ($^{230}\text{Th}/^{238}\text{U}$) = 0.96-0.97. The non-vesicular portions of sample MT75 have similar ratios between longer-lived U-series nuclides, with ($^{226}\text{Ra}/^{230}\text{Th}$) = 1.07-1.15, and ($^{230}\text{Th}/^{238}\text{U}$) = 0.95-0.97. However, ($^{210}\text{Pb}/^{226}\text{Ra})_0$ ratios are within error of equilibrium (**Fig. 7**). The vesiculated interior of MT75 has significantly lower ($^{230}\text{Th}/^{238}\text{U}$) and higher ($^{226}\text{Ra}/^{230}\text{Th}$) ratios (**Fig. 7**) than the non-vesiculated portion. Importantly, the ($^{210}\text{Pb}/^{226}\text{Ra})_0$ ratios of the two vesiculated samples differ, with ($^{210}\text{Pb}/^{226}\text{Ra})_0 = 0.8$ to 1.2 (**Fig. 6C and 7**).

5. Discussion

5.1. Millennial-scale magma additions and decadal-scale volatile fluxes

Disequilibria between isotopes in the ^{238}U decay chain constrains timescales of magmatic processes such as mantle melting or addition of slab fluids (e.g. Turner et al., 2003). Disequilibria are measurable for up to approximately 5 half-lives of the daughter isotope (Bourdon et al., 2003) although errors are considerably larger after 2-3 half-lives have passed. Unusually for recent arc magmas, most SHV andesite samples have equilibrium ($^{230}\text{Th}/^{238}\text{U}$) and ($^{226}\text{Ra}/^{230}\text{Th}$) ratios (**Fig. 6A-B, Fig. 7**). If the parental magmas for this system have U-Th-Ra disequilibrium, as is suggested by the enclave data presented here and in McGee et al. (2019), then these data are consistent with the mass accumulation of the bulk andesite over hundreds of thousands of years (^{230}Th half-life = 75 kyrs) without significant additional U-Th-Ra fractionation (Zellmer et al., 2003a). This scenario might be expected for thawing of an older plutonic mush (Cooper and Kent, 2014) or long timescales of melt residence in the lower to middle crust. Although melting of upper crustal plutonics beneath SHV is unlikely given their recent generation (<170 ka), hydrothermally altered volcanic rocks from the 550-950 ka Centre Hills Volcano are present in the subsurface (Paulatto et al., 2019). Some Phase I andesite samples have ($^{234}\text{U}/^{238}\text{U}$) ratios >1 (McGee et al. 2019) which may support interaction with hydrothermally altered rocks (due to the preferential loss of ^{234}U upon interaction with fluid). This interpretation is consistent with hydrogen isotope evidence cited in Harford and Sparks (2001) for

remelting of altered material in Phase I amphiboles. Nevertheless, the significant U- and Ra-excesses in most enclave samples at SHV (**Fig. 6A-B, Fig. 7**) show that young mafic magmas have intruded into the andesite within millennia of eruption (^{226}Ra half-life = 1600 yrs). This places a time constraint on mafic magma recharge into the andesitic magma system over its lifespan.

The much shorter half-lives involved in the ^{226}Ra - ^{222}Rn - ^{210}Pb portion of the ^{238}U decay chain (^{210}Pb half-life = 22.6 years, ^{222}Rn half-life = 3.8 days) mean that ratios of these isotopes can detect and constrain timescales of magmatic processes occurring over several decades prior to eruption. The relatively consistent $(^{210}\text{Pb}/^{226}\text{Ra})_0$ values of 1.4 for samples from enclave MT35 show enrichment in Rn or Pb over Ra shortly before it erupted. In contrast, enclave MT75 must have been subject to a complex history of short-lived radionuclide migration based on the mixed $(^{210}\text{Pb}/^{226}\text{Ra})_0$ values in samples from the vesicular interior and the equilibrium values for the non-vesicular portion (**Figs. 6-7**). The $(^{210}\text{Pb}/^{226}\text{Ra})_0$ value of 1 for the host andesite, however, show that, whatever its cause, this signature was not imparted to the andesite. Increasingly large ^{210}Pb -deficits in the andesite erupted from 1995 to 2010 were modelled by McGee et al. (2015) to reflect continuous degassing of ^{222}Rn from the andesitic reservoir over several decades. Similar deficits of ^{210}Pb with respect to ^{226}Ra due to year to decade scale degassing are common in basaltic lavas from non-arc settings (e.g. Kilauea, Girard et al., 2017; Mt Cameroon, Turner et al., 2013).

5.2. The potential of Pb contribution from old and young crystals

There is abundant petrographic evidence for transfer of material between andesite and enclave magmas (**Section 4.1**) and several studies have documented crystal exchange from andesite to enclave magma and vice versa specifically in material from the most recent SHV eruptions (Barclay et al., 2010; Humphreys et al., 2010; 2013; Murphy et al., 2000; Plail et al., 2014a). **Figures 2 and 3** show a range of plagioclase sizes in MT35 and MT75 which we interpret as the transfer of older, inherited phenocrysts into the mafic magma sourcing the enclaves and younger material from the mafic enclave present in the host andesite. Importantly, although disaggregation of enclaves clearly takes place (a study by Humphreys et al. (2013) calculated that approximately 16% of andesite groundmass plagioclase may have come from the mafic enclaves), there is no record of ^{210}Pb -excess transfer from the enclave to the andesite in contact during disaggregation, at least on a timescale that can be reflected in ^{226}Ra - ^{210}Pb disequilibria.

The relative proportion and location of plagioclase populations that are potentially the last to have formed ('younger') and all other plagioclase ('older') is portrayed in **Figure 2**. While groupings of plagioclase are in reality far more complex, this classification aids discussion of possible sources of young Pb. Given the small slices of each sample analysed for this study, it is possible that some

sections contained larger amounts of phenocrysts than others. A cross-polarised light view of each sample was chosen where enclave-andesite proportions were similar; we note that not all plagioclase is included due to very small grain size or extinction position, therefore populations represent a minimum estimate. Plagioclase phenocrysts generally larger than 1 mm with sieve textures, complex oscillatory zoning and frequently composed of several glomerocrysts were labelled as ‘older’ (**Fig. 2**). This population is very common in the andesite, less common in the enclave and rare in the vesicular enclave of MT75. A plagioclase population characterised by euhedral lath-shaped crystals prevalently <1 mm in length in general lacking sieve textures was labelled as ‘younger’. Obvious rims on ‘older’ plagioclase cores were also classed as ‘younger’ plagioclase (**Fig. 2**). Both younger rims and phenocrysts are far less common in the andesite than in the enclave portions of both samples (modal proportions using ImageJ are shown in the **online appendix**). These populations are observed in the XRF trace element map of Al, Ca and Fe (**Fig. 3**) which shows abundant plagioclase phenocrysts (orange) in each andesite portion of the two samples which are present in the enclave portions rimmed with, presumably younger, material (yellow). The vesicular section of the enclave in MT75 contains less of this material and more lath-shaped, higher Ca microphenocrysts of plagioclase (as seen on **Figure 3**).

Accumulation of plagioclase has the potential to affect whole rock $(^{210}\text{Pb}/^{226}\text{Ra})_0$ ratios because partition coefficients for Pb are higher than those for Ra in plagioclase. Residence times of some plagioclase phenocrysts in the andesite are in the century to millennia scale based on element diffusion profiles (Zellmer et al., 2002b), and therefore will have equilibrium $(^{210}\text{Pb}/^{226}\text{Ra})_0$ ratios. Potentially of more significance are crystals grown within a few decades of the eruption i.e. on the timescale of ^{226}Ra - ^{210}Pb decay. Indeed, young plagioclase separates from Mt St Helens, Merapi and Arenal volcanoes all have high $(^{210}\text{Pb}/^{226}\text{Ra})_0$ ratios (4.4, 1.97 and 1.8 respectively, Handley et al., 2018; Reagan et al., 2008; Reagan et al., 2006). Ultimately, however, Pb and Ra are both incompatible in plagioclase at the anorthite compositions encountered in the samples presented here (Bindeman, 2007; Bindeman et al., 1998; Tepley et al., 2010). Thus, any reasonable amount of plagioclase accumulation would have little effect on the bulk rock $(^{210}\text{Pb}/^{226}\text{Ra})_0$ values and we assume that the majority of Pb and Ra are hosted in glass.

5.3. Contribution of Pb from magmatic volatile phases and sulphide melts

A more promising explanation for the ^{210}Pb -excesses in the enclaves is the transfer of ^{222}Rn (e.g. Condomines et al., 2010) or ^{210}Pb itself into the enclave magmas during interaction with a MVP before the enclaves were included in the andesite magma. Water contents for mafic magmas feeding into the SHV system at approximately 10 km depth are at least 6 wt% decreasing to c. 2 wt%

in the andesite due to MVP saturation and loss (Edmonds et al., 2014). CO₂ likely makes up about 50 mol% of the MVP, and S gases are a few mol% (based on the exsolved vapour of Edmonds et al. 2014). Chlorine concentrations decrease from c. 4 wt% to 2 wt% as water decreases from 6 to 0.5 wt% for melt inclusions in plagioclase and orthopyroxene in the andesite, showing that the MVPs generated at depth are Cl-bearing (Edmonds et al., 2014). During decompression MVPs can separate into a higher salinity brine and a lower salinity, but sulphur enriched, vapour phase (e.g. Heinrich et al., 1999; Nadeau et al., 2016), both of which are more buoyant than the surrounding igneous mushes and magma (Richards, 2011; Sparks et al., 2019). Direct measurement of vapour (hydrous fluid) and brines trapped in melt inclusions has shown that metals (e.g. Cu, Pb, Zn) and some incompatible elements (e.g. Ba) are more compatible in MVPs compared to silicate melt (Heinrich et al., 1999; Lowenstern et al., 1991; Zajacz et al., 2008). Here we use the term MVP to include both hydrous fluid and any higher salinity brine that may be present.

Whole rock S abundance (**Fig. 5**) in the samples is relatively low (tens of ppm) compared with typical arc melt inclusion values of several hundreds of ppm for basalts and andesites (e.g. Nadeau et al., 2013), which is consistent with S partitioning into MVPs coexisting with the melt (Edmonds et al., 2014). A broad, negative association between S and Cu (**Table 1**) indicates that Cu is not complexed with S in the magma sourcing the enclaves and may be complexed instead with Cl. S-Cl decoupling has been observed in gas emission studies at SHV (Christopher et al., 2010). Cu and Pb/Ba correlate positively with $(^{210}\text{Pb}/^{226}\text{Ra})_0$ (**Fig. 8A-B**) ($r^2 = 0.8$ when MT75B with low ^{226}Ra is not included), which is suggestive of a recent enrichment in Cu and Pb by interaction with an MVP. The andesite samples have low Cu and Pb/Ba contents, although some local andesites are highly enriched in both Pb and Cu (Plail et al., 2014b). As the $(^{210}\text{Pb}/^{226}\text{Ra})_0$ ratios of 0.8-0.9 (^{210}Pb -deficits) in these samples are likely to be a result of continuous degassing of ^{222}Rn from the andesitic reservoir (**Section 5.1**, McGee et al., 2019), it is probable that the andesite did not interact with an MVP by the same mechanisms as hypothesised for the enclave magma.

In addition to their affinity for MVPs, ore metal elements can also be affected by interaction with immiscible sulphides and fractional crystallisation. Thorium is incompatible in most volcanic mineral phases, sulphide melts and volatiles (e.g. Bacon and Druitt, 1988; Zajacz et al., 2008). It is therefore a good indicator of magmatic evolution through fractional crystallisation. Amphibole and plagioclase crystallisation vectors are plotted on **Figures 8 C-F** to illustrate 10, 20 and 30% crystallisation, although, consistent with previous work (see **Section 5.1-5.2**), we note that the magmas are substantially mixed and therefore simple fractional crystallisation may be unrealistic. The compositional effect of sulphide crystallisation is shown in **Figures 8 C-F** as a schematic vector,

deduced based on the K_D of Cu between sulphide and basaltic melt from Ripley et al. (2002) and assuming that the relative K_{DS} involved are $Cu > Pb > Th > Ba, Dy$ and Yb in sulphides. An indicative vector denoting addition or expulsion (loss) of a metal-bearing MVP was calculated based on K_{DS} for both hydrous fluids and brines in granitic melts (from Zajacz et al. 2008), and for fluids in mafic melts (from Guo and Audétat, 2017). An estimated fluid composition was calculated by multiplying the partition coefficient by a potential melt composition, a primitive basalt from South SHV, MVO139 in Zellmer et al. (2003a). Mixing lines were then constructed between the fluid and melt. Details of all models and assumptions are given in the **online appendix**. Although not quantitative due to the lack of measured K_{DS} for all elements and unknown melt and fluid compositions, partitioning of Cu into MVPs produces distinct trends in **Figures 8 C-F**. Copper behaves compatibly in the enclave samples (Cu decreases with increasing Th), while it behaves incompatibly in the andesite samples (**Figs. 8C-F**) (Cu increases with increasing Th). The compositional separation of the enclave and andesite samples is also observed in Pb/Ba vs. Cu (**Fig. 8C**), with the positive trend of the enclaves lying at higher Pb/Ba than the andesite samples. The positive trend can be explained by extraction of an MVP which is richer in Cu than Pb as magmas fractionate from basaltic andesite to andesite, then continued differentiation of the andesite primarily by crystal fractionation alone. Data from SHV samples from Phase I (1997) and Phase V (2010) with available trace elements plotted on **Figure 8** are consistent with the trends observed in samples MT35 and MT75.

Thus, the differentiation between enclave-like magma and the host andesite appears to have been affected by loss of an MVP in addition to fractionation by crystallisation of minerals or sulphides. Expulsion of the MVP may have driven crystallisation through second boiling, that is, the saturation and exsolution of volatiles due to the crystallisation of anhydrous minerals (*cf.* Edmonds and Woods, 2018), which is also consistent with the diktytaxitic texture observed (**Section 4.1, Fig. 3**). Although trace element concentrations and U-series isotopic ratios in serially sliced MT35 (**Fig. 1A**) have a stepwise change from enclave to andesite (**Figs. 5 and 7**) the first sample of the andesite (MT35-D) has consistently higher incompatible element contents (Ba, Pb and Th in **Figure 5**, and see **Table 1**). This suggests that melt expelled from the enclave may have concentrated at the enclave-host andesite interface. Enclaves with the highest Cu and $(^{210}Pb/^{226}Ra)_0$ may represent some retention of an MVP-enriched melt. Although vectors for sulphide crystallisation follow similar trends to MVP expulsion, we favour the explanation of Edmonds et al. (2014) of loss of an MVP derived from evidence in melt inclusions of coupled Cl and water degassing.

Cu abundances of 30-80 ppm (**Table 1, Fig. 5**) are typical for arc-type andesites and basalts (see Nadeau et al. (2013) for a global compilation of Cu, Pb and Zn abundances). Despite this, and the low

whole rock S in the samples, volatile interaction has imparted signatures on the samples (**Fig. 8**) which can be linked to transfer of MVPs at different levels of the magmatic system at SHV. Given the very large SO₂ plume emitted throughout the 1995-2010 AD eruptions (continuing until the present day) these generally low abundances indicate very efficient segregation of volatiles from depth. Plail et al. (2014b) identified fracture zones within the andesite with elevated metal concentrations (Cu up to 200 ppm), which provide evidence of metal transport in the recent eruptions at SHV. Recent numerical models by Lamy-Chappuis et al. (2020) show that tubes may develop in crystalline mushes at a critical volatile volume. This could be a highly efficient means of transporting metals to the surface at SHV, given that estimates of exsolved vapor within a deeper magma are as much as 4.2 – 8.2 vol % at c. 30 km below the edifice (Edmonds et al., 2011). Similar veins of high metal concentrations were identified at Chaiten and Cordon Caulle (Berro et al., 2013; Paisley et al., 2019) and interpreted as channels of gas transport. Despite the metal transport in these veins during these eruptions, gas transport did not impart ²¹⁰Pb-excess here either, which is attributed to the sustained high flux of gas required to impart ²¹⁰Pb-excess (Paisley et al. 2019).

5.4. Two-step interaction between magmatic components of the SHV system and metal-carrying volatiles

In a study of SHV melt inclusions and phenocrysts Edmonds et al. (2014) proposed that volatiles erupted with the andesite magma originated from mafic magma recharge. It was hypothesised that volatile transfer/transport occurred either by vesiculation and entrainment of bubbles at the ‘hybrid’ layer (the interface between mafic and andesitic reservoirs *cf.* Plail et al., 2018), or by inclusion and subsequent disaggregation of enclaves into the andesite. Our study shows that significant inmixing of disaggregated enclaves (i.e. more than already hypothesised by Humphreys et al. (2009)) shortly before eruption is unlikely; given the presence of ²¹⁰Pb-deficits in the andesite instead of ²¹⁰Pb-excesses. Our results support that the MVPs originate from fractionation of deeper mafic magma to generate the host andesite, and the application of U-series isotopes provides important constraints on the degree of interaction between the magmatic reservoirs at SHV, their ability to transport metals and the timescales involved.

We suggest a two-step interaction between deeper mafic magma (not seen), the interface between mafic and andesitic magma which is the source of the enclaves, and the andesite. **Figure 9** shows the hypothesised isotopic and elemental characteristics of the potential magmatic components. A deeper mafic magma intruding at approximately 10 km depth (Christopher et al., 2015) is likely recently formed due to the presence of ²³⁸U-²³⁰Th-²²⁶Ra-²¹⁰Pb disequilibria in the mafic enclaves. The enclaves are formed at an interface between the mafic magma and the accumulated mass of

andesite. Melt and MVPs from the mafic magma are rapidly passed to the interface, and enclaves formed transport ^{210}Pb - and ^{226}Ra -excesses plus relative enrichments of Cu and S which may be transferred to pathways/veins within the andesite (*c.f.* Plail et al., 2018). The majority of MVP transfer from the deeper mafic magma to the interface, however, bypasses the andesite reservoir and is degassed from the magmatic system, suggesting that simple transfer of volatiles from enclaves into andesite did not trigger the current eruption. The broad grouping of U-series disequilibria with sample type (andesite vs. enclave) emphasises the ‘stepped’ interaction between magmatic reservoirs (**Figs. 8-9**). Enclaves with ^{210}Pb -excess represent parts of an interface that retains the signature of volatile fluxing. We suggest that the interior, vesicular portion of sample MT75 (**Fig. 1B**) represents a part of the interface where volatile flux and expulsion is more chaotic (**Fig. 9**). Although it is not possible to distinguish whether enclaves were formed through forced injection, volatile-induced gravitational instability or syn-eruptive inclusion (**Section 2**), the time between transfer of Rn and/or Pb from the mafic magma to the enclave magma and subsequent enclave eruption must have been on the scale of decades to maintain ($^{210}\text{Pb}/^{226}\text{Ra}$) excesses in the enclaves (**Fig. 7**). This short timescale and lack of a volatile enriched signature in the andesite could support a syn-eruptive origin of the SHV enclaves as hypothesised by Plail et al. (2018) and may require an external eruption trigger. Previous magmatic unrest episodes in 1897, 1933-38, 1966 and 1991 (Wadge and Isaacs, 1988) could also represent some mass (including volatile) transfer. It is possible that indicators of metal transport (such as the negative correlation between Cu and Th in **Fig. 8D**) may be more pronounced in eruptive Phases I and II where a more continuous addition of mafic magma at depth has been hypothesised (Barclay et al., 2010; McGee et al., 2019). Variations in concentrations involving Cu, Th and Pb/Ba between enclaves and andesites (**Fig. 8**) indicate that an MVP was lost during magma evolution through crystal fractionation from basaltic andesite to andesite. Although the small but progressive ^{210}Pb deficits in the andesite (McGee et al., 2019) indicate that degassing of the andesite reservoir took place during the recent eruptive phase of SHV, near equilibrium U-Th-Ra ratios in the andesite samples strongly indicate that the andesite was assembled over timescales of tens to hundreds of thousands of years or more. This is consistent with the general model of Blundy et al. (2015) where long-lived accumulation of arc magmatic intrusions over tens to hundreds of thousands of years is destabilised on a much shorter timescale.

6. Conclusions

The detailed application of U-series isotopes across the andesite-enclave interface of samples from the most recent eruption at Soufrière Hills Volcano, Montserrat has revealed important insights into the role of volatiles in eruption triggering and metal transport. The enclave samples represent parts

of the interface between a deeper mafic magma and the andesitic reservoir feeding eruptions. Equilibrium U-Th-Ra ratios in the andesite suggest it accumulated magma over several hundreds of thousands of years, while Ra-excesses of the enclaves suggest that the deeper, recharge magma is several thousands of years old. ^{210}Pb -excesses in most of the enclave samples are interpreted as due to interaction with a magmatic volatile phase originating from deeper, mafic magma that is transferred and mainly expelled from the system (within decades, i.e. on the scale of the eruption itself), although we note that some of this melt remains at the interface with the andesite on individual enclave samples. Concurrent magma evolution at the interface between andesite and mafic magma through crystal fractionation may occur due to the expulsion of the MVP. The andesite magma, which is in Pb-Ra equilibrium or ^{210}Pb -deficit, is either affected by MVP interaction on a timescale undetectable by Pb-Ra systematics (<2 years, Reagan et al., 2018) or does not interact with MVPs, leading us to question the role that recharge magma has on the trigger of eruptions at SHV. The application of short-lived isotopes at SHV has shown that the timescales involved in the transport of economically important elements may be related to only certain levels of a magmatic system. Additional studies on this topic may aid understanding of the efficiency of transport and eventual concentration of arc-related ore bodies.

Acknowledgments

This study was funded by an Australian Research Council (ARC) Discovery Project grant (DP150100328). HH was supported by an ARC Future Fellowship (FT120100440). At MQGA Peter Wieland and Sean Murray are thanked for trace element analyses, Olivier Alard for volatile element analyses and Tim Murphy for help with the MicroXRF. LM acknowledges support from the Mineral Exploration Cooperative Research Centre whose activities are funded by the Australian Government's Cooperative Research Centre Program. The coherency of this study was improved by comments from Silvio Mollo and an anonymous reviewer, and editor Balz Kamber is warmly thanked for his editorial handling.

Figure and table captions:

Figure 1: Photographs of the two samples analysed for this study. Both are from the 2010 eruption of Soufrière Hills Volcano

Figure 2: Relative proportions and locations of plagioclase populations for each sample using cross polarised light (XPL) images. Images were selected to show approximately equal amounts of enclave,

andesite and vesicular enclave in the case of MT75. Relatively ‘younger’ plagioclase phenocrysts and microphenocrysts were identified from the above XPL images based on their lath-like shape and general lack of sieve textures, and as rims on older crystals. ‘Older’ plagioclase crystals were categorised based on their agglomerated shape, sieve textures and oscillatory zoning, and in the enclave portion are assumed to be mainly inherited from the host andesite. Not all plagioclase are imaged due to their small size (microlites are not taken into account) or those in extinction in the image.

Figure 3: Polished thin section X-ray maps for Al, Ca and Fe abundance from the two samples in this study. Plagioclase is the most abundant mineral and is mainly rich in Al and Ca (orange in colour with red and green patchy areas) in each host andesite portion of the MT75 and MT35 samples, which are present as well in the basalt andesite enclaves. Orthopyroxene minerals (blue) are often mantled by clinopyroxene rims (green) and amphibole is rich in Fe and Ca (blue and green). Boundaries between enclaves and andesite are marked by dashed lines. Textures and mineral contents in the andesite and enclave portion of each sample are similar, while the interior part of the enclave in MT75 is more vesicular and contains less large, zoned (older inherited) crystals. BA = basaltic andesite

Figure 4: Multielement plot for andesites and enclave samples from MT35 and MT75 normalised to the primitive mantle values of Sun and McDonough (1989). The most mafic basalt from the 100 ka South Soufrière Hills volcano (‘South SHV basalt’) is plotted for comparison (MVO-139 from Zellmer et al. 2003a). Andesite samples are more enriched than enclaves in the most incompatible elements, but similar in Pb, Sr and HREE except for one MT35 andesite sample.

Figure 5: Selected trace element and whole rock volatile data (C-N-S) for sample MT35 (left panel) and MT75 (right panel). Data points for MT35 represent serially sliced samples (see **Figure 1A**) and are clustered by region in MT75 for trace elements to represent the sample locations (vesicular enclave (A & B), normal enclave (C & D) and andesite (E)) rather than a set of serial samples, as shown in **Figure 1B**. The multiple aliquots measured for each sample are shown for C-N-S. Error bars on selected elements reflect accuracy on the standards (see **Section 3.2**).

Figure 6: A: U-Th disequilibria, **B:** Th-Ra disequilibria and **C:** age-corrected Ra-Pb disequilibria of the studied serial sections (data in colour) compared to enclave and andesite data from 1995 to 2010 (data in black and white) from McGee et al. 2019. The maximum 2σ error bar is shown in A as it is similar for all samples. Individual 2σ error bars are shown for all new data in B and C. Grey lines marked S.E in B and C = secular equilibrium. MT75 samples are denoted by an asterisk within the symbols.

Figure 7: U-series activity ratios for sample MT35 (left panel) and MT75 (right panel). Data point layout is as for **Figure 5**. S.E = secular equilibrium. Error bars on all ratios are 2σ , except for ($^{226}\text{Ra}/^{230}\text{Th}$) in MT75 which is the 5% offset on the standard for these data (**Section 3.3, online appendix**)

Figure 8: U-series and elemental plots of both samples MT35 and MT75. Note the similar trends in ($^{210}\text{Pb}/^{226}\text{Ra}$)₀ vs. Cu (**A**) and Pb/Ba (**B**). Tick marks on fractional crystallisation vectors for plagioclase and amphibole in **C-F** denote 10% crystallisation increments with the exception of amphibole in **E** ('amph*') where tick marks denote 5% increments. Partition coefficients used are from Luhr and Carmichael (1980), Brenan et al. (1995), Liu et al. (2015), Bacon and Druitt (1988) and Ewart and Griffin (1994). The sulphide fractionation vector in **D-F** is based on the assumption that $\text{Cu} > \text{Pb} > \text{Th} \gg \text{Ba}$, Dy and Yb in sulphides ($K_D\text{Cu} = 480\text{-}1303$, Ripley et al. (2002)), and is indicative rather than calculated. Black solid and dashed lines labelled 'MV' indicate the potential effect of addition or expulsion (loss) of a magmatic volatile phase and are inferred from partition coefficients between melts and vapours and brines from Zajacz et al. (2008) and Guo and Audétat (2017). A 10% error bar is shown on Cu to reflect accuracy on the standards, internal precision is <4% (see **Section 3.2**). 'Other 1995-2010 SHV' are from Phases I and V, ($^{210}\text{Pb}/^{226}\text{Ra}$)₀ in **A** and **B** are from McGee et al. (2019) and trace element data from Zellmer et al (2003a) and Plail et al. (2014a). See **online appendix** for full details of partition coefficients, assumptions and models.

Figure 9: Schematic illustrating the magmatic system interactions at SHV deduced from data in this study, incorporating trace element variations and timescale information from U-series isotopes. Not to scale. See discussion.

Table 1: All trace element, U-series and volatile element data for the samples presented in this study. All trace element data and volatile element data are in ppm. Parentheses denote activity ratios, ($^{210}\text{Pb}/^{226}\text{Ra}$)₀ is corrected for age of eruption. All data, duplicates and standards are presented in the online appendix.

References

Bacon, C.R., 1986. Magmatic inclusions in silicic and intermediate volcanic rocks. *Journal of Geophysical Research: Solid Earth*, 91(B6): 6091-6112.

- Bacon, C.R., Druitt, T.H., 1988. Compositional evolution of the zoned calcalkaline magma chamber of Mount Mazama, Crater Lake, Oregon. *Contributions to Mineralogy and Petrology*, 98(2): 224-256.
- Barclay, J., Herd, R.A., Edwards, B.R., Christopher, T., Kiddle, E.J., Plail, M., Donovan, A., 2010. Caught in the act: Implications for the increasing abundance of mafic enclaves during the recent eruptive episodes of the Soufrière Hills Volcano, Montserrat. *Geophysical Research Letters*, 37(19).
- Berlo, K., Tuffen, H., Smith, V.C., Castro, J.M., Pyle, D.M., Mather, T.A., Geraki, K., 2013. Element variations in rhyolitic magma resulting from gas transport. *Geochimica et Cosmochimica Acta*, 121: 436-451.
- Berlo, K., Turner, S., 2010. ^{210}Pb – ^{226}Ra disequilibria in volcanic rocks. *Earth and Planetary Science Letters*, 296(3–4): 155-164.
- Bindeman, 2007. Erratum to IN Bindeman, AM Davis, and M. Drake (1998), Ion microprobe study of plagioclase-basalt partition experiments at natural concentration levels of trace elements, *Geochimica Cosmochimica Acta* 62, 1175: 1193. *Geochimica et Cosmochimica Acta*, 71(9): 2414-2414.
- Bindeman, I.N., Davis, A.M., Drake, M.J., 1998. Ion microprobe study of plagioclase-basalt partition experiments at natural concentration levels of trace elements. *Geochimica et Cosmochimica Acta*, 62(7): 1175-1193.
- Blondes, M.S., Reiners, P.W., Duce, M.N., Singer, B.S., Chesley, J., 2008. Temporal-compositional trends over short and long time-scales in basalts of the Big Pine Volcanic Field, California. *Earth and Planetary Science Letters*, 269: 140-154.
- Blundy, J., Mavrogenes, J., Tattitch, B., Sparks, S., Gilmer, A., 2015. Generation of porphyry copper deposits by gas-brine reaction in volcanic arcs. *Nature Geosci*, 8(3): 235-240.
- Bourdon, B., Turner, S., Henderson, G.M., Lundstrom, C.C., 2003. Introduction to U-series Geochemistry. *Reviews in Mineralogy and Geochemistry*, 52(1): 1-21.
- Brenan, J., Shaw, H., Ryerson, F., Phinney, D., 1995. Experimental determination of trace-element partitioning between pargasite and a synthetic hydrous andesitic melt. *Earth and Planetary Science Letters*, 135(1-4): 1-11.

- Christopher, T., Blundy, J., Cashman, K., Cole, P., Edmonds, M., Smith, P., Sparks, R., Stinton, A., 2015. Crustal-scale degassing due to magma system destabilization and magma-gas decoupling at Soufrière Hills Volcano, Montserrat. *Geochemistry, Geophysics, Geosystems*, 16(9): 2797-2811.
- Christopher, T., Edmonds, M., Humphreys, M., Herd, R.A., 2010. Volcanic gas emissions from Soufrière Hills Volcano, Montserrat 1995–2009, with implications for mafic magma supply and degassing. *Geophysical Research Letters*, 37(19).
- Cioni, R., Civetta, L., Marianelli, P., Metrich, N., Santacroce, R., Sbrana, A., 1995. Compositional Layering and Syn-eruptive Mixing of a Periodically Refilled Shallow Magma Chamber: the AD 79 Plinian Eruption of Vesuvius. *Journal of Petrology*, 36(3): 709–76.
- Condomines, M., Sigmarsson, O., Gauthier, P.J., 2010. A simple model of ^{222}Rn accumulation leading to ^{210}Pb excesses in volcanic rocks. *Earth and Planetary Science Letters*, 293(3–4): 331-338.
- Coombs, M.L., Eichelberger, J.C., Rutherford, M.J., 2003. Experimental and textural constraints on mafic enclave formation in volcanic rocks. *Journal of Volcanology and Geothermal Research*, 119(1): 125-144.
- Cooper, K.M., Kent, A.J., 2014. Rapid remobilization of magmatic crystals kept in cold storage. *Nature*, 506(7489): 480.
- Edmonds, M., Brett, A., Herd, R.A., Humphreys, M.C.S., Woods, A., 2015. Magnetite-bubble aggregates at mixing interfaces in andesite magma bodies. Geological Society, London, Special Publications, 410(1): 95-121.
- Edmonds, M., Humphreys, M.C., Hauri, E.H., Herd, R.A., Wadge, G., Rawson, H., Ledden, R., Plail, M., Barclay, J., Aiuppa, A., 2014. Pre-eruptive vapour and its role in controlling eruption style and longevity at Soufrière Hills Volcano. Geological Society, London, Memoirs, 39(1): 291-315.
- Edmonds, M., Woods, A.W., 2018. Exsolved volatiles in magma reservoirs. *Journal of Volcanology and Geothermal Research*.
- Eichelberger, J.C., Izbekov, P.E., 2000. Eruption of andesite triggered by dyke injection: contrasting cases at Karymsky Volcano, Kamchatka and Mt Katmai, Alaska. *Philosophical Transactions of the Royal Society of London. Series A: Mathematical, Physical and Engineering Sciences*, 358(1770): 1465-1485.

- Ewart, A., Griffin, W., 1994. Application of proton-microprobe data to trace-element partitioning in volcanic rocks. *Chemical Geology*, 117(1-4): 251-284.
- Gauthier, P.-J., Condomines, M., 1999. ^{210}Pb – ^{226}Ra radioactive disequilibria in recent lavas and radon degassing: inferences on the magma chamber dynamics at Stromboli and Merapi volcanoes. *Earth and Planetary Science Letters*, 172(1): 111-126.
- Girard, G., Reagan, M.K., Sims, K.W., Thornber, C.R., Waters, C.L., Phillips, E.H., 2017. ^{238}U – ^{230}Th – ^{226}Ra – ^{210}Pb – ^{210}Po Disequilibria Constraints on Magma Generation, Ascent, and Degassing during the Ongoing Eruption of Kīlauea. *Journal of Petrology*, 58(6): 1199-1226.
- Guo, H., Audétat, A., 2017. Transfer of volatiles and metals from mafic to felsic magmas in composite magma chambers: an experimental study. *Geochimica et Cosmochimica Acta*, 198: 360-378.
- Handley, H.K., Reagan, M., Gertisser, R., Preece, K., Berlo, K., McGee, L.E., Barclay, J., Herd, R., 2018. Timescales of magma ascent and degassing and the role of crustal assimilation at Merapi volcano (2006–2010), Indonesia: Constraints from uranium-series and radiogenic isotopic compositions. *Geochimica et Cosmochimica Acta*, 222(Supplement C): 34-52.
- Harford, C.L., Sparks, R.S.J., 2001. Recent remobilisation of shallow-level intrusions on Montserrat revealed by hydrogen isotope composition of amphiboles. *Earth and Planetary Science Letters*, 185(3): 285-297.
- Heinrich, C.A., Gunther, D., Audétat, A., Ulrich, T., Frischknecht, R., 1999. Metal fractionation between magmatic brine and vapor, determined by microanalysis of fluid inclusions. *Geology*, 27(8): 755-758.
- Humphreys, M., Edmonds, M., Christopher, T., Hards, V., 2010. Magma hybridisation and diffusive exchange recorded in heterogeneous glasses from Soufrière Hills Volcano, Montserrat. *Geophysical Research Letters*, 37(19).
- Humphreys, M., Edmonds, M., Plail, M., Barclay, J., Parkes, D., Christopher, T., 2013. A new method to quantify the real supply of mafic components to a hybrid andesite. *Contributions to Mineralogy and Petrology*, 165(1): 191-215.
- Humphreys, M.S., Christopher, T., Hards, V., 2009. Microlite transfer by disaggregation of mafic inclusions following magma mixing at Soufrière Hills volcano, Montserrat. *Contributions to Mineralogy and Petrology*, 157(5): 609-624.

- Kayzar, T.M., Cooper, K.M., Reagan, M.K., Kent, A.J.R., 2009. Gas transport model for the magmatic system at Mount Pinatubo, Philippines: Insights from $(^{210}\text{Pb})/(^{226}\text{Ra})$. *Journal of Volcanology and Geothermal Research*, 181(1): 124-140.
- Lamy-Chappuis, B., Heinrich, C.A., Driesner, T., Weis, P., 2020. Mechanisms and patterns of magmatic fluid transport in cooling hydrous intrusions. *Earth and Planetary Science Letters*, 535: 116111.
- Liu, X., Xiong, X., Audétat, A., Li, Y., 2015. Partitioning of Cu between mafic minerals, Fe–Ti oxides and intermediate to felsic melts. *Geochimica et Cosmochimica Acta*, 151: 86-102.
- Lowenstern, J.B., Mahood, G.A., Rivers, M.L., Sutton, S.R., 1991. Evidence for extreme partitioning of copper into a magmatic vapor phase. *Science*, 252(5011): 1405-1409.
- Luhr, J.F., Carmichael, I.S., 1980. The colima volcanic complex, Mexico. *Contributions to Mineralogy and Petrology*, 71(4): 343-372.
- Martin, V.M., Morgan, D.J., Jerram, D.A., Caddick, M.J., Frior, D.J., Davidson, J.P., 2008. Bang! Month-Scale Eruption Triggering at Santorini Volcano. *Science*, 321(5893): 1178.
- McGee, L., Reagan, M., Handley, H., Turner, S., Sparks, R.S., Berlo, K., Barclay, J., Turner, M., 2019. Volatile behaviour in the 1995–2010 eruption of the Soufrière Hills Volcano, Montserrat recorded by U-series disequilibrium in mafic enclaves and andesite host. *Earth and Planetary Science Letters*, 524: 115730.
- Murphy, M.D., Sparks, R.S.J., Barclay, J., Carroll, M.R., Brewer, T.S., 2000. Remobilization of Andesite Magma by Intrusion of Mafic Magma at the Soufriere Hills Volcano, Montserrat, West Indies. *Journal of Petrology*, 41(1): 21-42.
- Nadeau, O., Stix, J., Williams-Jones, A.E., 2013. The behavior of Cu, Zn and Pb during magmatic–hydrothermal activity at Merapi volcano, Indonesia. *Chemical Geology*, 342: 167-179.
- Nadeau, O., Stix, J., Williams-Jones, A.E., 2016. Links between arc volcanoes and porphyry-epithermal ore deposits. *Geology*, 44(1): 11-14.
- Paisley, R., Berlo, K., Ghaleb, B., Tuffen, H., 2019. Geochemical constraints on the role of tuffisite veins in degassing at the 2008–09 Chaitén and 2011–12 Cordón Caulle rhyolite eruptions. *Journal of Volcanology and Geothermal Research*, 380: 80-93.
- Pallister, J.S., Hoblitt, R.P., Reyes, A.G., 1992. A basalt trigger for the 1991 eruptions of Pinatubo volcano? *Nature*, 356: 426.

- Paulatto, M., Moorkamp, M., Hautmann, S., Hooft, E., Morgan, J.V., Sparks, R.S.J., 2019. Vertically extensive magma reservoir revealed from joint inversion and quantitative interpretation of seismic and gravity data. *Journal of Geophysical Research: Solid Earth*.
- Plail, M., Barclay, J., Humphreys, M.C., Edmonds, M., Herd, R.A., Christopher, T.E., 2014a. Characterization of mafic enclaves in the erupted products of Soufrière Hills Volcano, Montserrat, 2009 to 2010. *Geological Society, London, Memoirs*, 39(1): 343-360.
- Plail, M., Edmonds, M., Humphreys, M.C.S., Barclay, J., Herd, R.A., 2014b. Geochemical evidence for relict degassing pathways preserved in andesite. *Earth and Planetary Science Letters*, 386: 21-33.
- Plail, M., Edmonds, M., Woods, A.W., Barclay, J., Humphreys, M.C.S., Herd, R.A., Christopher, T., 2018. Mafic enclaves record syn-eruptive basalt intrusion and mixing. *Earth and Planetary Science Letters*, 484: 30-40.
- Reagan, M.K., Cooper, K.M., Pallister, J.S., Thornber, C.R., Wortel, M., 2008. Timing of degassing and plagioclase growth in lavas erupted from Mount St. Helens, 2004-2005, from ^{210}Po - ^{210}Pb - ^{226}Ra disequilibria: Chapter 37 in *A volcano rekindled: the renewed eruption of Mount St. Helens, 2004-2006*. 1750-37, Reston, VA.
- Reagan, M.K., Tepley, F.J., Gill, J.B., Wortel, M., Garrison, J., 2006. Timescales of degassing and crystallization implied by ^{210}Po - ^{210}Pb - ^{226}Ra disequilibria for andesitic lavas erupted from Arenal volcano. *Journal of Volcanology and Geothermal Research*, 157(1-3): 135-146.
- Richards, J.P., 2011. Magmatic to hydrothermal metal fluxes in convergent and collided margins. *Ore Geology Reviews*, 40(1): 1-26.
- Ripley, E.M., Brophy, J.G., Li, C., 2002. Copper solubility in a basaltic melt and sulfide liquid/silicate melt partition coefficients of Cu and Fe. *Geochimica et Cosmochimica Acta*, 66(15): 2791-2800.
- Ruprecht, P., Bachmann, O., 2010. Pre-eruptive reheating during magma mixing at Quizapu volcano and the implications for the explosiveness of silicic arc volcanoes. *Geology*, 38(10): 919-922.
- Rusk, B.G., Reed, M.H., Dilles, J.H., Klemm, L.M., Heinrich, C.A., 2004. Compositions of magmatic hydrothermal fluids determined by LA-ICP-MS of fluid inclusions from the porphyry copper-molybdenum deposit at Butte, MT. *Chemical Geology*, 210(1): 173-199.

- Sigmarrsson, O., Vlastelic, I., Andreasen, R., Bindeman, I., Devidal, J.L., Moune, S., Keiding, J.K., Larsen, G., Höskuldsson, A., Thordarson, T., 2011. Remobilization of silicic intrusion by mafic magmas during the 2010 Eyjafjallajökull eruption. *Solid Earth*, 2(2): 271-281.
- Sparks, R., Marshall, L., 1986. Thermal and mechanical constraints on mixing between mafic and silicic magmas. *Journal of Volcanology and Geothermal Research*, 29(1-4): 99-124.
- Sparks, R.S.J., Annen, C., Blundy, J.D., Cashman, K.V., Rust, A.C., Jackson, M.D., 2019. Formation and dynamics of magma reservoirs. *Philosophical Transactions of the Royal Society A: Mathematical, Physical and Engineering Sciences*, 377(2139): 20180019.
- Sun, S.-s., McDonough, W.F., 1989. Chemical and isotopic systematics of oceanic basalts: implications for mantle composition and processes. Geological Society, London, Special Publications, 42(1): 313-345.
- Suzuki, Y., Yasuda, A., Hokanishi, N., Kaneko, T., Nakada, S., Fujii, T., 2013. Syneruptive deep magma transfer and shallow magma remobilization during the 2011 eruption of Shinmoe-dake, Japan—Constraints from melt inclusions and phase equilibria experiments. *Journal of Volcanology and Geothermal Research*, 257: 184-204.
- Tepley, F.J., Lundstrom, C.C., McDonough, W.F., Thompson, A., 2010. Trace element partitioning between high-An plagioclase and basaltic to basaltic andesite melt at 1 atmosphere pressure. *Lithos*, 118(1): 82-94.
- Thomas, N., Tait, S., 1997. The dimensions of magmatic inclusions as a constraint on the physical mechanism of mixing. *Journal of Volcanology and Geothermal Research*, 75(1-2): 167-178.
- Turner, M.B., Reagan, M.K., Turner, S.P., Sparks, R.S.J., Handley, H.K., Girard, G., Suh, C.E., 2013. Timescales of magma degassing — Insights from U-series disequilibria, Mount Cameroon, West Africa. *Journal of Volcanology and Geothermal Research*, 262(0): 38-46.
- Turner, S., Bourdon, B., Gill, J., 2003. Insights into Magma Genesis at Convergent Margins from U-series Isotopes. *Reviews in Mineralogy and Geochemistry*, 52(1): 255-315.
- Ubide, T., Galé, C., Larrea, P., Arranz, E., Lago, M., Tierz, P., 2014. The Relevance of Crystal Transfer to Magma Mixing: a Case Study in Composite Dykes from the Central Pyrenees. *Journal of Petrology*, 55(8): 1535-1559.

- Wadge, G., Isaacs, M.C., 1988. Mapping the volcanic hazards from Soufriere Hills Volcano, Montserrat, West Indies using an image processor. *Journal of the Geological Society*, 145(4): 541-551.
- Wadge, G., Voight, B., Sparks, R., Cole, P., Loughlin, S., Robertson, R., 2014. An overview of the eruption of Soufriere Hills Volcano, Montserrat from 2000 to 2010. Geological Society, London, *Memoirs*, 39(1): 1-40.
- Zajacz, Z., Halter, W.E., Pettke, T., Guillong, M., 2008. Determination of fluid/melt partition coefficients by LA-ICPMS analysis of co-existing fluid and silicate melt inclusions: controls on element partitioning. *Geochimica et Cosmochimica Acta*, 72(8): 2169-2197.
- Zellmer, G.F., Hawkesworth, C.J., Sparks, R.S.J., Thomas, L.E., Harford, C.L., Brewer, T.S., Loughlin, S.C., 2003a. Geochemical Evolution of the Soufrière Hills Volcano, Montserrat, Lesser Antilles Volcanic Arc. *Journal of Petrology*, 44(8): 1349-1374.
- Zellmer, G.F., Sparks, R.S.J., Hawkesworth, C.J., Wiedenbeck, M., 2003b. Magma Emplacement and Remobilization Timescales Beneath Montserrat: Insights from Sr and Ba Zonation in Plagioclase Phenocrysts. *Journal of Petrology*, 44(8): 1413-1431.

Declaration of interests

The authors declare that they have no known competing financial interests or personal relationships that could have appeared to influence the work reported in this paper.

The authors declare the following financial interests/personal relationships which may be considered as potential competing interests:

Journal Pre-proof

Sample name	MT35-A	MT35-B	MT35-C	MT35-D	MT35-E	MT35-F	MT75-A	MT75-B	MT75-C	MT75-D	MT75-E
Sample type	Enclave	Enclave	Enclave	Andesite	Andesite	Andesite	Ves. enclave	Ves. enclave	Enclave	Enclave	Andesite
Sc	31.4	30.9	31.4	22.0	16.4	18.7	38.1	37.4	26.8	27.2	13.9
Ti	4951	4848	5049	4555	3411	3884	5573	5466	4722	4623	3409
V	243	242	244	173	134	151	274	268	221	218	112
Cr	16	13	17	10	11	12	17	17	15	15	12
Mn	1363	1321	1342	1560	1248	1428	1226	1208	1327	1338	1308
Co	25	24	25	20	15	17	72	0	79	87	138
Ni	12	11	11	6	5	5	16	15	11	11	7
Cu	66	69	68	42	33	36	77	62	43	30	48
Zn	68	66	69	71	58	64	62	62	64	65	61
Ga	17.5	17.4	17.9	17.9	16.2	16.6	17.7	17.4	17.6	17.6	16.5
Rb	8.1	7.8	9.2	16.7	14.1	15.9	6.8	8.2	9.4	9.5	17.5
Sr	283	282	289	277	262	260	277	274	281	276	267
Y	22	21	22	30	21	23	21	22	21	22	23
Zr	57	55	59	84	75	79	56	66	67	70	86
Nb	2.26	1.70	1.87	2.27	2.55	2.79	1.45	1.59	1.90	2.04	3.15
Cs	0.29	0.28	0.30	0.30	0.52	0.57	0.24	0.29	0.34	0.35	0.61
Ba	102	101	108	207	184	189	77	96	121	130	223
La	6.3	6.0	6.5	11.2	9.6	9.9	4.8	5.4	7.0	7.1	11.2
Ce	14.1	14.1	15.1	25.5	20.6	22.3	12.2	13.3	16.2	16.7	24.2
Pr	2.0	2.0	2.1	3.5	2.7	2.9	1.8	1.9	2.2	2.3	3.1
Nd	9.3	9.1	9.6	15.3	11.1	12.3	8.5	8.9	9.8	10.0	12.8
Sm	2.6	2.5	2.7	3.9	2.7	3.1	2.5	2.6	2.5	2.6	3.0
Eu	0.89	0.88	0.92	1.17	0.91	0.98	0.89	0.89	0.90	0.90	1.00
Tb	0.50	0.49	0.52	0.72	0.47	0.54	0.51	0.52	0.49	0.50	0.53
Gd	3.02	2.95	3.11	4.30	2.90	3.28	3.05	3.10	2.91	3.05	3.23
Dy	3.20	3.15	3.35	4.46	2.98	3.38	3.30	3.36	3.06	3.23	3.31
Ho	0.71	0.69	0.73	1.00	0.66	0.76	0.73	0.73	0.68	0.71	0.73
Er	2.04	2.00	2.14	2.92	1.95	2.32	2.09	2.12	1.99	2.07	2.17

Yb	2.00	1.94	2.07	2.94	2.04	2.29	1.97	2.02	1.98	2.05	2.28
Lu	0.31	0.31	0.32	0.46	0.33	0.36	0.31	0.31	0.32	0.32	0.37
Hf	1.57	1.51	1.63	2.37	1.98	2.14	1.52	1.70	1.76	1.83	2.27
Ta	0.18	0.12	0.12	0.22	0.21	0.20	0.20	0.20	0.24	0.28	0.49
Pb	2.32	2.26	2.44	2.90	2.52	2.68	1.68	1.95	2.28	2.28	3.41
*Th	1.22 ± 0.01	1.14 ± 0.01	1.24 ± 0.01	2.42 ± 0.03	2.34 ± 0.03	2.44 ± 0.03	0.84 ± 0.01	1.03 ± 0.01	1.46 ± 0.02	1.51 ± 0.02	2.75 ± 0.03
*U	0.38 ± 0.004	0.36 ± 0.004	0.39 ± 0.004	0.75 ± 0.008	0.73 ± 0.008	0.76 ± 0.008	0.28 ± 0.003	0.34 ± 0.004	0.47 ± 0.005	0.48 ± 0.005	0.87 ± 0.01
*Ra fg/g	143 ± 3.2	141 ± 3.1	155 ± 3.4	258 ± 5.7	251 ± 5.5	257 ± 5.7	118 ± 2.6	192 ± 4.3	161 ± 3.6	185 ± 4.1	284 ± 6.3
(²³⁴U/²³⁸U)	1.002 ± 0.004	1.004 ± 0.004	1.004 ± 0.004	1.003 ± 0.004	0.998 ± 0.004	1.009 ± 0.005	1.001 ± 0.004	0.999 ± 0.004	0.997 ± 0.004	1.003 ± 0.004	1.002 ± 0.004
(²³⁸U/²³²Th)	0.936 ± 0.015	0.963 ± 0.015	0.962 ± 0.015	0.945 ± 0.015	0.953 ± 0.015	0.941 ± 0.015	1.006 ± 0.016	1.012 ± 0.016	0.978 ± 0.016	0.965 ± 0.015	0.956 ± 0.015
(²³⁰Th/²³²Th)	0.903 ± 0.005	0.931 ± 0.006	0.930 ± 0.006	0.933 ± 0.006	0.938 ± 0.006	0.931 ± 0.006	0.917 ± 0.006	0.923 ± 0.006	0.928 ± 0.006	0.931 ± 0.006	0.935 ± 0.006
(²³⁰Th/²³⁸U)	0.964 ± 0.017	0.967 ± 0.017	0.967 ± 0.017	0.987 ± 0.016	0.975 ± 0.016	0.989 ± 0.016	0.912 ± 0.018	0.912 ± 0.017	0.949 ± 0.017	0.965 ± 0.017	0.979 ± 0.016
(²²⁶Ra/²³⁰Th)	1.153 ± 0.027	1.179 ± 0.027	1.196 ± 0.027	1.05 ± 0.023	1.016 ± 0.023	1.007 ± 0.023	1.375 ± 0.031	1.813 ± 0.041	1.065 ± 0.025	1.181 ± 0.027	0.991 ± 0.022
(²¹⁰Pb/²²⁶Ra)₀	1.374 ± 0.191	1.448 ± 0.182	1.303 ± 0.172	0.829 ± 0.097	0.870 ± 0.124	-	1.275 ± 0.225	0.755 ± 0.143	1.044 ± 0.277	0.872 ± 0.230	1.049 ± 0.161
S range	38-46	44-52	36-57	29-30	24-30	30-36	32-45	44-72	39-61	45-66	42-53
C range	262- 265	176- 224	202- 230	190- 225	103- 122	293- 325	467- 518	409- 429	1122- 1566	485- 571	422- 556
N range	222	190- 191	263	287	241- 242	279	102- 118	82- 167	175- 316	156- 209	168- 380

*Isotope dilution analysis